Porphyrin−Silicon Hybrid Field-Effect Transistor with Individually Addressable Top-gate Structure
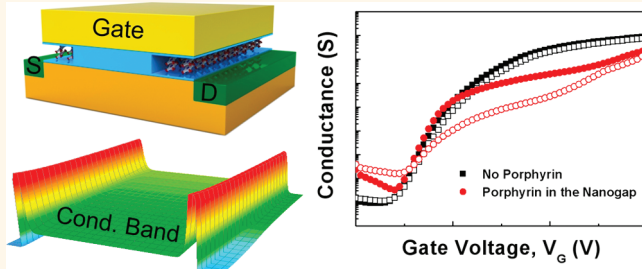
Myeong-Lok Seol, Sung-Jin Choi, Chang-Hoon Kim, Dong-Il Moon, and Yang-Kyu Choi*

Department of Electrical Engineering, KAIST, 291 Daehak-ro, Republic of Korea

The hybrid integration of inorganic semiconductors and organic molecules has been widely investigated for exploratory nanodevices.[1−20] In particular, photoactive molecules on a semiconductor interface have been studied intensively for the purpose of implementing optically controlled electronic devices.[6−18] The photoactive hybrid devices have shown unique and interesting optical phenomena that a single type device alone cannot have. High carrier mobility and reproducible behavior can be achieved because of its single-crystalline inorganic channel, while high photosensitivity and charge containing characteristics can also be achieved due to the organic molecules. Porphyrin, a crucial component of chlorophyll, is one of the most attractive photoactive molecules. Its high environmental stability and reliable photoinduced charge transfer (PCT) characteristics make the porphyrin the best counterpart for hybrid devices.[14] Various semiconductor−porphyrin composites have been investigated for the purpose of studying the mechanism of charge transfer and applying the knowledge to optoelectronic nanodevices.[9−18]

Most early analyses of porphyrin composites focused on carbon−porphyrin interactions using carbon nanotubes or fullerenes. The analyses explored the fast charge separation and slow recombination states of carbon−porphyrin composites and attempted to implement the composites in various device applications, such as optically controlled memory and optical switches.[9−13] However, isolating the charge transfer effect in carbon−porphyrin composites was difficult because the molecules can also induce an unwanted chemical doping effect. Furthermore, the organic semiconductor channel suffered from difficulties in doping and chirality control; in addition, an unwanted Schottky barrier

ABSTRACT

A conductance-controllable hybrid device that utilizes the photoinduced charge transfer behavior of a porphyrin in a field-effect transistor (FET) with a nanogap is proposed and analyzed. A conventional metal-oxide-semiconductor (MOS) structure is modified to form a nanogap in which the porphyrin can be embedded. The conductance of an inversion channel is controlled by the negatively charged, optically activated porphyrin molecules. The proposed nanogap-formed MOSFET structure solves the conventional dilemma that a top-gate cannot be used for an organic−inorganic hybrid device because the top-gate blocks an entire area of a channel where organic material should be immobilized. The top-gate structure has much practicality compared with the back-gate structure because each device can be controlled individually. Furthermore, the device is highly compatible with the chip-based integrated system because the fabrication process follows the standard complementary metal-oxide-semiconductor (CMOS) technology. The charge transfer mechanisms between silicon and porphyrin are analyzed using devices with different doping polarities and geometrical parameters. The results show that the influence of the negative charge of the porphyrin in the device is reversed when opposite doping polarities are used. The device characteristics can be comprehensively evaluated using the energy band diagram analysis and simulation. The possible application of the proposed device for nonvolatile memory is demonstrated using the optical charging and electrical discharging behavior of the porphyrins.

KEYWORDS: organic−inorganic hybrid device · field-effect transistor (FET) · porphyrin · molecular device · nanogap · photoinduced charge transfer (PCT)

inevitably developed between the probing pad and the channel. In contrast, it is easy to dope a silicon channel and control the doping polarity, and the formation of a Schottky contact is not always necessary. Above all, silicon devices have a large advantage in terms of practicality due to its well-established fabrication techniques. Hence, recent studies have focused on
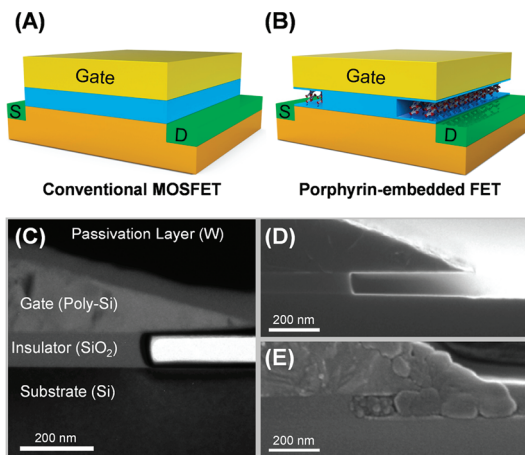
the hybrid integration of porphyrin—silicon hybrid devices.[14—18]

Regardless of the channel material, one-dimensional nanowire structures have been widely used in organic—inorganic hybrid devices.[3,4,6—8,13,15,18] Some devices used a simple two-terminal nanowire resistor; others used a back-gated three-terminal nanowire field-effect transistor (FET). A three-terminal FET type provides benefits from its multifaceted functionality and versatile modes of operation. However, only a back-gate can be implemented for the nanowire FET because the body of the nanowire must be opened for any subsequent immobilization of molecules. Yet, in spite of its fabrication simplicity, the back-gate structure has a critical weakness in practicality; it cannot control a device individually because the electric field induced by the back-gate is applied to the entire wafer. In this study, we embed porphyrin in the nanogap of a top-gate silicon FET. Because the individual device can be controlled independently, it is compatible with mass production and an integrated circuit such as a commercialized system-on-a-chip (SoC) and lab-on-a-chip system. The results confirm that porphyrin plays a significant role in determining the conductance of an inversion channel.

RESULTS AND DISCUSSION

The structure of the porphyrin-embedded FET is similar to the conventional metal-oxide-semiconductor FET (MOSFET), as shown in Figure 1A,B. In a conventional MOSFET, the conduction channel is continuously formed under the gated region and allows the electrons or holes to flow freely. In a FET with a nanogap, however, as the electrons encounter a discontinuous channel under the region where the nanogap is formed, the conductance of the channel is significantly reduced. The nanogap creates a region that acts as a potential barrier that suppresses the current flow in the channel. Consequently, the amount of external charge inside the nanogap becomes important in determining the channel conductance because the charge controls the potential barrier of the conduction channel. Therefore, the charged state of the porphyrins inside the nanogap plays an important role in determining the conductance of the device. Transmission electron microscope (TEM) and scanning electron microscope (SEM) images confirmed that the nanogap was well formed and the porphyrins filled the nanogap well (Figure 1C—E). In this experiment, the drop-casting method was used to introduce the porphyrins into the nanogap. Because the metal top-gate can reduce the intensity of the incident light, polycrystalline silicon heavily doped with n-type dopants (abbreviated as n+ polysilicon) was used rather than a metal gate.
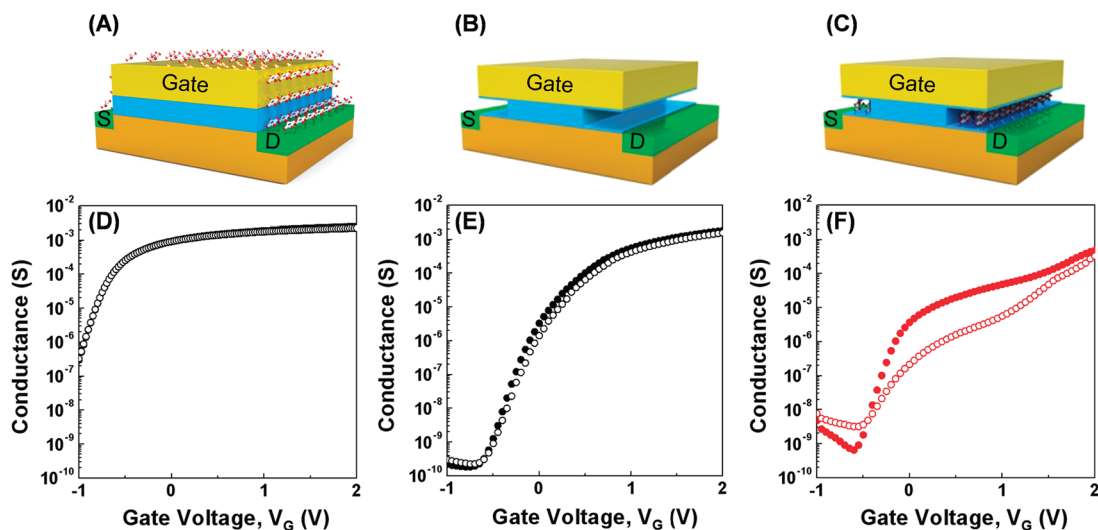
To confirm the operation principle, we fabricated three samples for the control experiments: a device

Figure 1. (A) Schematic of a conventional MOSFET (B) Schematic of a porphyrin-embedded FET. (C) Transmission electron microscopy (TEM) image of the fabricated FET with a nanogap without embedded porphyrin. The triangular shape of the gate is caused by isotropic etching of wet chemicals. All scale bars indicate 200 nm. (D) Scanning electron microscope (SEM) image of the FET with a nanogap without embedded porphyrin. (E) SEM image of the porphyrin-embedded FET.

with the porphyrin attached but without the nanogap (Figure 2A), a device with a nanogap but without porphyrin (Figure 2B), and a device with porphyrin embedded in the nanogap (Figure 2C). The device with porphyrin but no nanogap had the conduction characteristic that was almost identical to those of the conventional MOSFET (Figure 2D). The threshold voltage was smaller than that of the other samples because the electric field from the gate affected the conduction channel through the intact SiO_2 layers. After 20 s of light illumination, the conductance of the channel was not changed. From this result, we can conclude that the porphyrins attached outside of the nanogap such as on the gate, source, and drain did not significantly affect the device. For the device with only the nanogap, the absolute value of the conductance was smaller than the conventional MOSFET due to the potential barrier under the nanogap region (Figure 2E). After 20 s of light illumination, the conductance only slightly decreased. This slight decrement was due to the exposed SiO_2 in the nanogap because the SiO_2 can act as an electron acceptor at the $Si—SiO_2$ interface.[21] The porphyrin-embedded nanogap device, which is the object of this study, showed substantial reduction of the conductance after the light illumination. From the direction of the conductance change, we can infer that porphyrin tends to be negatively charged when illuminated by light.[18] The negatively charged porphyrin in the nanogap partially repels the inversion electrons, causing a decrease in the channel conductance.

The mechanism of conductance change of the inversion channel was interpreted using energy band diagram analysis (Figure 3A). The 3D band diagrams of

Figure 2. (A–C) Schematics of the control and experimental devices to determine the effect of the porphyrins in the nanogap: device with (A) porphyrin only, (B) nanogap only, and (C) both porphyrin and the nanogap, (D–F) Conductance *versus* the gate voltage characteristic before (filled dot) and after (hollow dot) light illumination of the device with (D) porphyrin only, (E) nanogap only, and (F) both porphyrin and the nanogap. The filled points were measured in a stabilized dark condition, and the hollow points were measured in a dark condition immediately after 20 s of illumination (1.22 mW/mm², halogen lamp).
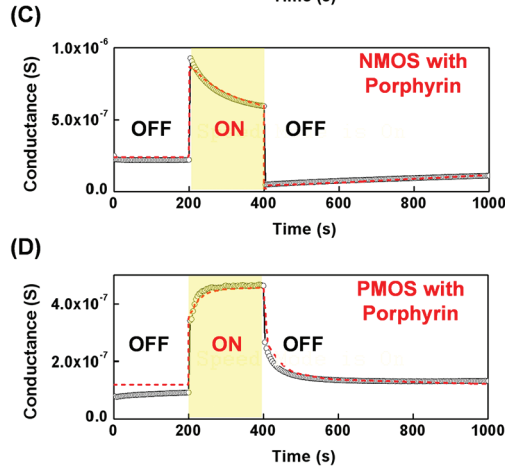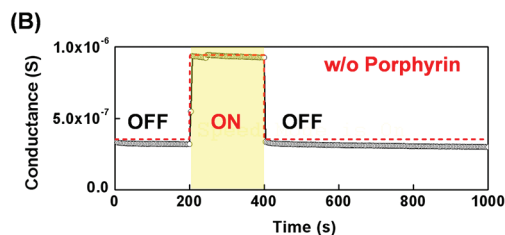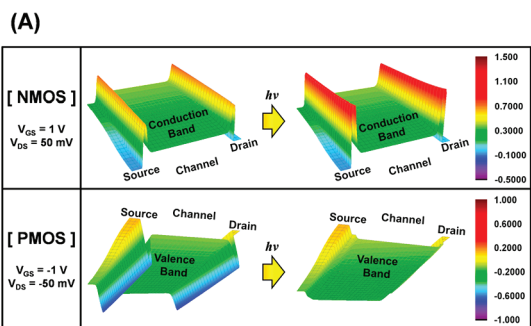
the devices were extracted from the commercialized semiconductor simulator (ATLAS/Silvaco).[22] The validity of the ATLAS tool for analyzing organic–silicon hybrid devices was first verified by Takulapalli *et al.*[23] For an n-channel FET (NMOS), whose major carriers are electrons, the potential barrier at the conduction band determines the conductance. When the porphyrin is exposed to light, it absorbs electrons and becomes negatively charged. The absorbed electrons are derived from the silicon body because there are many electron–hole pairs created as a result of the optical generation process. The electron transport behavior is based on PCT, which was reported in our previous work analyzing the interaction between silicon nanowires and porphyrins.[18] These negative charges repel electrons from the channel and increase the potential barrier height. Thus, the electrons cannot easily flow through the potential barrier, and the decreased conductance is observed as a result. On the other hand, in a p-channel FET (PMOS), whose major carriers are holes, the potential barrier at the valence band determines the conductance. Therefore, as the porphyrin becomes negatively charged from the light illumination, holes can be easily formed in the channel, and the potential barrier becomes smaller. See the Supporting Information for the detailed simulation procedure.

This expected polarity dependency was confirmed from transient analyses using simulation and experimental measurement (Figure 3B–D). The dashed line shows the simulation results of the device, and the hollow dots show the measured data. The well-known MOSFET behavior was evident in the reference group (Figure 3B); because light generates electron–hole pairs, the conductance increased and was sustained during the illumination. After the light was turned off,

the conductance rapidly returned to its normal state. In contrast, when porphyrin was embedded in the nanogap of the n-channel FET, the conductance continued to fall throughout the illumination, which means that the porphyrin absorbed electrons from the channel increasingly with time (Figure 3C). The porphyrin sustained the light-induced charged state for several tens of minutes even after the light was turned off, and it slowly returned to its original state afterward. When porphyrin was embedded in the nanogap of a p-channel FET, the conductance increased, as expected, when the device was illuminated (Figure 3D). After the light was turned off, the conductance remained at this increased level for a while and eventually returned to its original value.
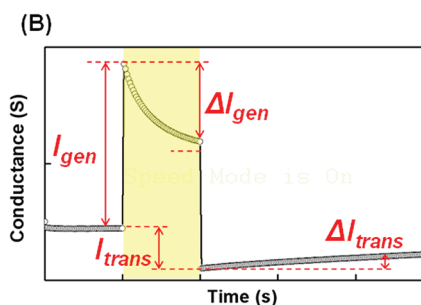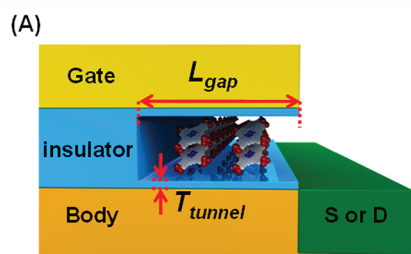
Figure 4A shows a magnified schematic of the nanogap region. The geometry of the nanogap was determined from several process parameters: nanogap height was determined by the thickness of the initial gate insulator; nanogap length (L_{gap}) was determined by the etching time on the insulator; and the surrounding tunneling oxide thickness (T_{tunnel}) was determined by the temperature and time of the thermal reoxidation process. Figure 4B illustrates the definitions of the analysis parameters using a transient graph of the n-channel porphyrin-embedded FET: the generation current (I_{gen}) is the increment in current immediately after illumination; the delta generation current (ΔI_{gen}) is the change in current during illumination; the transition current (I_{trans}) is the difference in current before and after illumination; and the delta transition current (ΔI_{trans}) is the amount of current recovered after the light is turned off.

To clarify the relationship between the nanogap length and the total conductance, we fabricated devices with various nanogap lengths (L_{gap}). Figure 5A

(A)

(B)

(C)

(D)
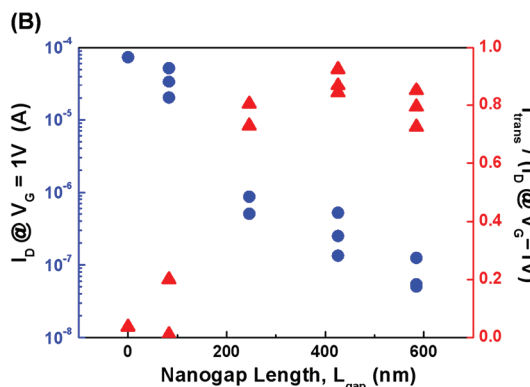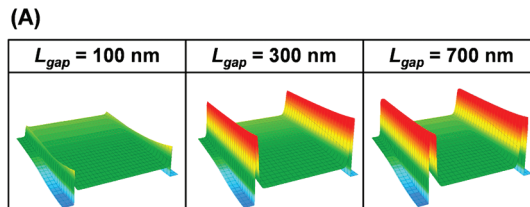
Figure 3. (A) Three-dimensional simulation results of band diagram along the channel for the n-channel FET (NMOS) and p-channel FET (PMOS). The illuminated porphyrin causes the barrier to be higher for the NMOS but lower for the PMOS. The color map represents the energy level of the band edge. (B) Transient characteristic of the FET without porphyrin. Hollow dots represent measurement data, and red dashed line represents simulation results. The yellow background indicates the illumination time (1.22 mW/mm^2, halogen lamp). The gate voltage was 0.5 V. (C) Transient characteristic of the n-channel porphyrin-embedded FET. The gate voltage was 0.5 V. (D) Transient characteristics of the p-channel porphyrin-embedded FET. The gate voltage was −0.5 V.

shows the band diagrams from the ATLAS simulation of the porphyrin-embedded FET with different nanogap lengths. As the nanogap length increases, both the height and length of the potential barrier were increased. Figure 5B shows the absolute value of the current (I_D) at a fixed gate voltage and the current reduction ratio (I_{trans}/I_D). The absolute current value decreased with nanogap length because, as shown in Figure 5A, the width and height of the potential barrier are increased. In contrast, the light-induced current reduction ratio increases with a longer nanogap. Because the current is reduced by the porphyrin

(A)

(B)
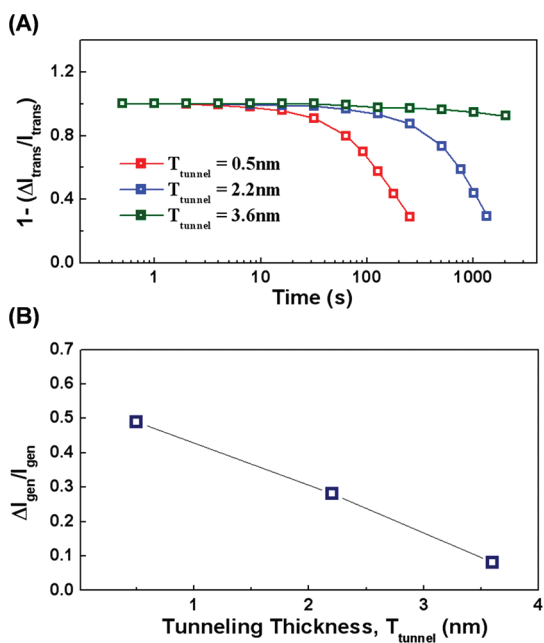
Figure 4. (A) Magnified schematic of the nanogap region to define the tunneling thickness (T_{tunnel}) and the nanogap length (L_{gap}). (B) Transient graph defining the parameters: I_{gen}, ΔI_{gen}, I_{trans}, and ΔI_{trans}.

(A)

(B)

Figure 5. (A) Three-dimensional simulation results of conduction band of the n-type porphyrin-embedded FET devices with various nanogap lengths. The potential barrier becomes higher and longer as the nanogap length increases. (B) Absolute current value for a gate voltage of 1 V (primary y-axis, blue circle points) and the current change ratio during illumination (secondary y-axis, red square points) as functions of nanogap length.
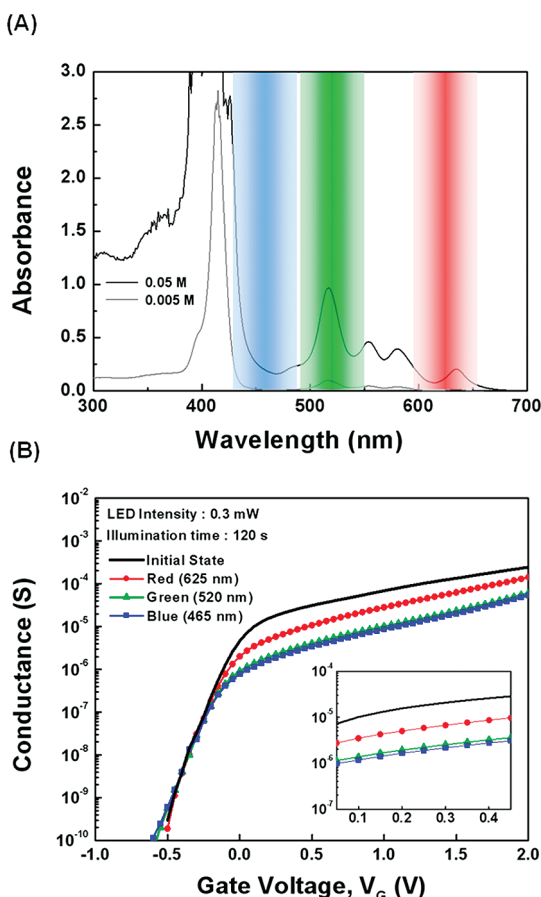
embedded in the nanogap, the larger volume of porphyrin in the longer nanogap produces a greater sensitivity to external light. However, when the nanogap length exceeds 500 nm, the initial conductance before the illumination is so small that the negative charge of the porphyrin cannot significantly change the conductance.

(A)

(B)

Figure 6. (A) Charge retention characteristics as a function of tunneling thickness (T_{tunnel}). The dotted lines on the x-axis indicate the time constant of the charge retention. (B) Charge absorption as a function of tunneling thickness. The y-axis shows the amount of normalized current change during 200 s of illumination. The amount of the current change decreases as the tunneling distance increases.

The electron transfer process was examined for various oxide thicknesses between the porphyrin and the silicon body (T_{tunnel}). The charge retention time of the porphyrin increased when a thicker oxide was used (Figure 6A). However, in terms of the charge transfer efficiency, porphyrin absorbs electrons faster when a thinner oxide was used (Figure 6B). This trade-off relationship can be simply interpreted as a well-known tunneling mechanism; when the barrier is wide, the electrons cannot easily tunnel into or out of the nanogap region. This result is consistent with the results of a previous study on a charge transfer through a molecule−silicon interface.[24]
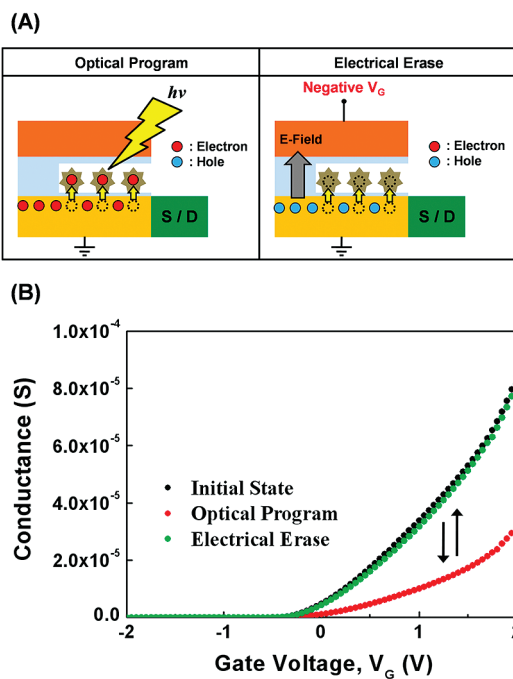
Optical responses from different wavelengths were measured and compared with the UV−visible spectra of the porphyrin. Three light-emitting diodes (LEDs) were used with center wavelengths of 625, 520, and 465 nm. The wavelength spectra follow a Gaussian profile with a tail-to-tail width of approximately 100 nm. The UV−visible spectra of the porphyrin show a strong responses to the Soret and Q-band (Figure 7A), as shown by previous reports.[18,25] The spectrum of the blue LED includes the edge of the Soret band, the green LED includes the center of the Q-band, and the red LED includes the edge of the Q-band. The expected absorption efficiency in the UV−visible spectrum and the measured results of the transfer characteristics are well matched (Figure 7B). The change in conductance is the smallest for the red LED, whereas the green and blue LEDs show approximately twice larger changes

(A)

(B)

Figure 7. (A) UV−visible absorption spectrum of the porphyrin. The three color bars indicate the emission wavelengths of the light-emitting diodes (LEDs). (B) Transfer characteristics of the porphyrin-embedded FET when three different LEDs are illuminated. The center wavelengths of the each LED are 625, 520, and 465 nm. The intensity and duration of the illuminations are 0.3 mW/mm^2 and 120 s.

that are similar to one another. Although the absorption intensity of the Soret band is much stronger than that of the Q-band, the blue LED only includes part of the Soret band, while the green LED includes most of the Q-band. This wavelength dependency of porphyrin implies that the wavelength-dependent applications are possible with further optimization.

An important feature of the porphyrin-embedded FET is that the porphyrin holds its electrons for several tens of minutes. From the memory aspect, the charged state can be treated as a programmed state. When the device was illuminated, electron−hole pairs were generated and some of the electrons were absorbed by the porphyrin to produce the programmed state (Figure 8A). For a fast erase method, we used the electrical method that is used for conventional flash devices. When a negative gate pulse is applied, accumulated holes in the channel combine with the electrons within the porphyrin. This electron−hole recombination causes the device to switch to the erased state (Figure 8B).[3,4,26] We have confirmed these program and erase capabilities by analyzing the conductance−gate voltage characteristics

(A)

(B)

Figure 8. (A) Conceptual schematics of the mechanisms of the optical program and electrical erase characteristics. The porphyrin charging process is based on PCT, and the discharge process is based on electron–hole pair recombination. (B) Optical program (1.22 mW/mm^2, halogen lamp, 20 s) and electrical erase ($V_G = -7$ V, 1 ms) characteristics of the porphyrin-embedded FET.

(Figure 8C). The negative pulse can completely restore the conductance level to the initial state without causing any deformation or change in the electrical characteristics. Although the memory performance of the proposed porphyrin-embedded FET is currently poorer than commercial flash memory, the optical program method and the lower operation voltage are advantageous for low-power optoelectronic applications.

CONCLUSIONS

In summary, we have proposed and analyzed a porphyrin–silicon hybrid structure for the purpose of investigating an individually addressable top-gate molecular device. The top-gate FET structure has significant advantages in practicality and integrability because the conventional back-gate nanowire FET cannot be individually accessed when used in integrated chip-based applications, such as the SoC and lab-on-a-chip system. The conductance of an inversion channel was controlled by the PCT of the porphyrin. The porphyrin-embedded nanogap acted as a bottleneck for the creation of a conduction channel and thereby controlled the conductance. We found that the electron transfer process depends critically on the distance between the porphyrin and the silicon channel, which corresponds to the thickness of the tunneling oxide. In addition, we analyzed the impact of the nanogap length; longer nanogap produces a larger change in the conductance ratio. However, the absolute level of the conductance tends to be reduced, which is a disadvantage for the device operation. The porphyrin-embedded FET showed a weak response to red light, but the responses to the green and blue light were approximately twice as strong. This result is consistent with UV–visible absorption spectra. Finally, we demonstrated a possible application that the porphyrin-embedded FET can be used as an optically programmed nonvolatile memory.

METHODS

To fabricate the device, we first used basic silicon processing to make a conventional n-channel (p-type body and n+ source/drain) metal-oxide-semiconductor FET (MOSFET). The gate material was n+-doped polysilicon rather than metal to minimize the degradation of the incident light intensity. We then used a buffered oxide etchant (BOE) to carve a fraction of a SiO$_2$ layer, which serves as a gate insulator. After this etching process, the carved region formed a 100 nm high nanogap at the gate edges because the initial thickness of the gate oxide was 100 nm. The nominal gate length of the device was 10 μm, and the length of each nanogap (which was controlled by the BOE etching time) was approximately 250 nm after an etching time of 3 min. After the nanogap formation, thin SiO$_2$ was regrown on the channel interface using a thermal oxidation process. This regrown SiO$_2$ layer determines the tunneling distance between the silicon and porphyrin.

After the formation of the nanogap, we cast a 10 μL solution of a 1 mM tetra(4-sulfonatophenyl)porphyrin (TPPS, Sigma Aldrich) on the nanogap-formed FET. TPPS was used instead of normal porphyrin because of its better chemical binding properties and water solubility. A drop evaporation method was used for the porphyrin casting.[6,18,25] During a 12 h period of drying, porphyrin was inserted in the nanogap by capillary force. During this process, the porphyrin formed an agglomerated state and filled the entire nanogap space (Figure 1E).

Simulation of the band diagram and transient characteristics were conducted using commercial software (ATLAS/Silvaco). All device parameters were defined with the same values used for the real experimental device. For the n-channel devices (NMOS), the doping concentration of the body was 1×10^{16}/cm^3, and the polarity was p-type, whereas the doping concentrations of the source and drain were both 1×10^{20}/cm^3, and the polarity was n-type. For the p-channel devices (PMOS), the doping concentration was the same as the n-channel device (NMOS), but the polarity was reversed. The gate material was n-type polysilicon for the n-channel devices and p-type polysilicon for the p-channel devices. The gate length of the device was 10 μm, and the thickness of the gate oxide was 100 nm; these were the same as the experimental experiment. Porphyrins were modeled as a floating gate containing electrons. The charging and discharging rates were assumed to follow an exponential relationship, which was found to be reasonable because it matched the measured results well (Figure 3B–D). See the Supporting Information for more details of the simulation procedure.

Supporting Information Available: The ATLAS simulation procedure and the reproducibility experiments are described in the Supporting Information. This material is available free of charge *via* the Internet at http://pubs.acs.org.

REFERENCES AND NOTES

1. Aviram, A.; Ratner, M. A. Molecular Rectifiers. *Chem. Phys. Lett.* **1974**, *29*, 277–283.
2. Joachim, C.; Gimzewski, J. K.; Aviram, A. Electronics Using Hybrid-Molecular and Mono-Molecular Devices. *Nature* **2000**, *408*, 541–548.
3. Duan, X.; Huang, Y.; Lieber, C. M. Nonvolatile Memory and Programmable Logic from Molecule-Gated Nanowires. *Nano Lett.* **2002**, *2*, 487–490.
4. Li, C.; Ly, J.; Lei, B.; Fan, W.; Zhang, D.; Han, J.; Meyyappan, M.; Thompson, M.; Zhou, C. Data Storage Studies on Nanowire Transistors with Self-Assembled Porphyrin Molecules. *J. Phys. Chem. B* **2004**, *108*, 9646–9649.
5. Rakshit, T.; Liang, G.-C.; Ghosh, A. W.; Datta, S. Silicon-Based Molecular Electronics. *Nano Lett.* **2004**, *4*, 1803–1807.
6. Star, A.; Lu, Y.; Bradley, K.; Gruner, G. Nanotube Optoelectronic Memory Devices. *Nano Lett.* **2004**, *4*, 1587–1591.
7. Guo, X.; Huang, L.; O'Brien, S.; Kim, P.; Nuckolls, C. Directing and Sensing Changes in Molecular Conformation on Individual Carbon Nanotube Field Effect Transistors. *J. Am. Chem. Soc.* **2005**, *127*, 15045–15047.
8. Borghetti, J.; Derycke, V.; Lenfant, S.; Chenevier, P.; Filoramo, A.; Goffman, M.; Vuillaume, D.; Bourgoin, J.-P. Optoelectronic Switch and Memory Devices Based on Polymer-Functionalized Carbon Nanotube Transistors. *Adv. Mater.* **2006**, *18*, 2535–2540.
9. Imahori, H.; Hagiwara, K.; Aoki, M.; Akiyama, T.; Taniguchi, S.; Okada, T.; Shirakawa, M.; Sakata, Y. Linkage and Solvent Dependence of Photoinduced Electron Transfer in Zinc-porphyrin-C_{60} Dyads. *J. Am. Chem. Soc.* **1996**, *118*, 11771–11782.
10. Guldi, D. M. Fullerene-Porphyrin Architectures; Photosynthetic Antenna and Reaction Center Models. *Chem. Soc. Rev.* **2002**, *31*, 22–36.
11. Murakami, H.; Nomura, T.; Nakashima, N. Noncovalent Porphyrin-Functionalized Single-Walled Carbon Nanotubes in Solution and the Formation of Porphyrin-Nanotube Nanocomposites. *Chem. Phys. Lett.* **2003**, *378*, 481–485.
12. Li, H.; Zhou, B.; Lin, Y.; Gu, L.; Wang, W.; Fernando, K. A. S.; Kumar, S.; Allard, L. F.; Sun, Y.-P. Selective Interactions of Porphyrins with Semiconducting Single-Walled Carbon Nanotubes. *J. Am. Chem. Soc.* **2004**, *126*, 1014–1015.
13. Hecht, D. S.; Ramirez, R. J. A.; Briman, M.; Artukovic, E.; Chichak, K. S.; Stoddart, J. F.; Gruner, G. Bioinspired Detection of Light Using a Porphyrin-Sensitized Single-Wall Nanotube Field Effect Transistor. *Nano Lett.* **2006**, *6*, 2031–2036.
14. Liu, Z.; Yasseri, A. A.; Lindsey, J. S.; Bocian, D. F. Molecular Memories That Survive Silicon Device Processing and Real-World Operation. *Science* **2003**, *302*, 1543–1545.
15. Winkelmann, C. B.; Ionica, I.; Chevalier, X.; Royal, G.; Bucher, C.; Bouchiat, V. Optical Switching of Porphyrin-Coated Silicon Nanowire Field Effect Transistors. *Nano Lett.* **2007**, *7*, 1454–1458.
16. Shaw, J.; Zhong, Y.-W.; Hughes, K. J.; Hou, T.-H.; Raza, H.; Rajwade, S.; Bellfy, J.; Engstrom, J. R.; Abruna, H. D.; Kan, E. C. Integration of Self-Assembled Redox Molecules in Flash Memory Devices. *IEEE Trans. Electron Devices* **2010**, *58*, 826–834.
17. Wen, L.; Liu, X.; Yang, N.; Zhai, J.; Huang, C.; Li, Y.; Jiang, L. Photoelectric Conversion Behavior Based on Direct Interfacial Charge-Transfer from Porphyrin Derivative to Silicon Nanowires. *Appl. Phys. Lett.* **2010**, *97*, 253111.
18. Choi, S.-J.; Lee, Y.-C.; Seol, M.-L.; Ahn, J.-H.; Kim, S.; Moon, D.-I.; Han, J.-W.; Mann, S.; Yang, J.-W.; Choi, Y.-K. Bio-Inspired Complementary Photoconductor by Porphyrin-Coated Silicon Nanowires. *Adv. Mater.* **2011**, *23*, 3979–3983.
19. Otsuka, Y.; Naitoh, Y.; Matsumoto, T.; Mizutani, W.; Tabata, H.; Kawai, T. A Simple Fabrication Method of Nanogap Electrodes for Top-Contacted Geometry: Application to Porphyrin Nanorods and a DNA Network. *Nanotechnology* **2004**, *15*, 1639–1644.
20. Ogawa, T.; Ozawa, H.; Kawao, M.; Tanaka, H. Photo-Response Behavior of Au Nano-particle/Porphyrin Polymer Composite Device with Nano-Gapped Electrodes. *J. Mater. Sci.* **2007**, *18*, 939–942.
21. Mihaychuk, J. G.; Shamir, N.; van Driel, H. M. Multiphoton Photoemission and Electric-Field-Induced Optical Second-Harmonic Generation as Probes of Charge Transfer Across the Si/SiO_2 Interface. *Phys. Rev. B* **1999**, *59*, 2164–2173.
22. Silvaco International. ATLAS User's Manual Device Simulation Software. http://www.silvaco.com/.
23. Takylapalli, B. R.; Laws, G. M.; Liddell, P. A.; Andreasson, J.; Erno, Z.; Gust, D.; Thornton, T. J. Electrical Detection of Amine Ligation to a Metalloporphyrin *via* a Hybrid SOI-MOSFET. *J. Am. Chem. Soc.* **2008**, *130*, 2226–2233.
24. Mathur, G.; Gowda, S.; Li, Q.; Surthi, S.; Zhao, Q.; Misra, V. Monolayers on Thin Silicon Dioxide—A Study of the Dependence of Retention Time on Oxide Thickness. *IEEE Trans. Nanotechnol.* **2005**, *4*, 278–283.
25. Meadows, P. J.; Dujardin, E.; Hall, S. R.; Mann, S. Template-Directed Synthesis of Silica-Coated J-Aggregate Nanotapes. *Chem. Commun.* **2005**, *29*, 3688–3690.
26. Li, C.; Lei, B.; Fan, W.; Zhang, D.; Meyyappan, M.; Zhou, C. Molecular Memory Based on Nanowire-Molecular Wire Heterostructures. *J. Nanosci. Nanotechnol.* **2007**, *7*, 138–150.